Radio morphology-accretion mode link in FRII low-excitation radio galaxies

D. Macconi,[1,2]★, E. Torresi[2], P. Grandi[2], B. Boccardi[3] and C. Vignali[1,4]

[1]*Dipartimento di Fisica e Astronomia, Alma Mater Studiorum, Università degli Studi di Bologna, Via Gobetti 93/2, I-40129 Bologna, Italy*
[2]*INAF-Osservatorio di Astrofisica e Scienza dello Spazio di Bologna, Area della Ricerca CNR, Via Gobetti 101, I-40129 Bologna, Italy*
[3]*Max-Planck-Institut für Radioastronomie, Auf dem Hügel 69, D-53121 Bonn, Germany*
[4]*INAF-Osservatorio di Astrofisica e Scienza dello Spazio di Bologna, Via Gobetti 93/3, I-40129 Bologna, Italy*

ABSTRACT

Fanaroff-Riley II low-excitation radio galaxies (FRII-LERGs) are characterized by weak nuclear excitation on pc-scales and by properties typical of powerful FRIIs (defined as high-excitation, hereafter HERGs/BLRGs) on kp-scales. Since a link between the accretion properties and the power of the produced jets is expected both from theory and observations, their nature is still debated. In this work we investigate the X-ray properties of a complete sample of 19 FRII-LERGs belonging to the 3CR catalog, exploiting *Chandra* and XMM-*Newton* archival data. We also analyze 32 FRII-HERGs/BLRGs with *Chandra* data as a control sample. We compared FRII-LERG and FRII-HERG/BLRG X-ray properties and optical data available in literature to obtain a wide outlook of their behavior. The low accretion rate estimates for FRII-LERGs, from both X-ray and optical bands, allow us to firmly reject the hypothesis for that they are the highly obscured counterpart of powerful FRII-HERGs/BLRGs. Therefore, at least two hypothesis can be invoked to explain the FRII-LERGs nature: (i) they are evolving from classical FRIIs because of the depletion of accreting cold gas in the nuclear region, while the extended radio emission is the heritage of a past efficiently accreting activity; (ii) they are an intrinsically distinct class of objects with respect to classical FRIs/FRIIs. Surprisingly, in this direction a correlation between accretion rates and environmental richness is found in our sample. The richer the environment, the more inefficient is the accretion. In this framework, the FRII-LERGs are intermediate between FRIs and FRII-HERGs/BLRGs both in terms of accretion rate and environment.

Key words: galaxies: active – X-rays: galaxies – catalogues

1 INTRODUCTION

Black holes (BHs) inhabit the center of almost all massive galaxies and span a wide range of masses, from 10^6 $M_\odot$ to several 10^9 $M_\odot$, depending strongly on the properties of the host galaxy (Kormendy 1993; Magorrian et al. 1998; Gebhardt et al. 2000; Ferrarese & Merritt 2000; Tremaine et al. 2002; Kormendy 2004; Greene & Ho 2005, 2006; McConnell et al. 2011).

A small fraction of galaxies (~1%) show nuclear activity: they are called active galactic nuclei (AGN). AGN produce an enormous amount of energy in a tiny volume (<<pc) via gravitational accretion of matter onto the central BH. About 10% of AGN produce strong relativistic jets which emit non-thermal radiation over the (almost) whole electromagnetic spectrum, thus they are defined radio-loud AGN or *jetted* AGN (see Padovani 2016). Radio-loud AGN with strongly boosted emission associated to jets and pointing towards the observer's line-of-sight are called blazars. Conversely, radio-loud AGN whose jets are oriented close to the plane of the sky are called Radio Galaxies (RGs).

RGs were classified for the first time by Fanaroff & Riley (1974) following radio morphological criteria. Indeed, Fanaroff-Riley type one objects (FRI) show the highest surface brightness near the core along the jets (i.e. edge-darkened sources), while type two (FRII) objects are characterized by higher surface brightness at the lobes extremities, far from the nucleus (i.e. edge-brightened). There are some cases for which the morphological classification is ambiguous, e.g. they show FRII-like jets on one side and

★ E-mail: duccio.macconi2@unibo.it

FRI-like on the other: the so-called hybrid double sources (Gopal-Krishna & Wiita 2000).

The FRI-FRII morphological dichotomy quite neatly translates into a separation in terms of extended radio power: sources with radio luminosity at 178 MHz below 10^{26} W Hz^{-1} (Fanaroff & Riley 1974; Tadhunter 2016) are generally FRI, while sources with luminosity above this threshold tipically belong to FRII class.

RGs can be also classified on the basis of their optical spectra, accordingly to the emission lines produced in the Narrow Line Regions (hereafter NLR; Laing et al. 1994; Buttiglione et al. 2009, 2010, 2011), in High-Excitation or Low-Excitation Radio Galaxies (HERGs and LERGs, respectively). The main diagnostic of high excitation is the [OIII]λ5007 line luminosity. Conversely, the standard spectroscopic indicators of low excitation are [NII]λ6584, [SII]λ6716 and [OI]λ6364 (Buttiglione et al. 2010). To take into account simultaneously both high- and low-excitation diagnostics, Buttiglione et al. (2010) introduced the exctitation index (EI).[1] Considering that different excitation modes of the NLR are associated to different accretion rates (Gendre et al. 2013; Heckman & Best 2014), this spectroscopic classification reflects the accretion regime at work in the central regions of the AGN. In particular, HERGs accrete efficiently (quasar-mode, $L/L_{Edd} > 0.1$), i.e. the potential energy of the gas accreted by the super-massive black hole (SMBH) is efficiently converted into radiation (Narayan et al. 1998). Conversely, LERGs are characterized by low accretion rates typical of radiatively inefficient hot accretion flows (jet-mode, $L/L_{Edd} \leq 0.01$-0.1), and the jet carries the bulk of the AGN energy output (Narayan et al. 1998; Heckman & Best 2014).

Over the years, studies on radio-loud AGN were fundamental to investigate the jet-launching mechanism and the eventual connection between ejection of relativistic jets and accretion of material onto the central BH. Indeed, jets are produced close to the BH and their power is predicted to depend on the BH properties (mass and spin) and on the magnetic field strength: in Blandford & Znajek (1977a) model, the jet power (P_{jet}) is proportional to $(aMB)^2$, where a is the BH spin, M its mass and B is the magnetic field value at the BH horizon (Ghisellini et al. 2014).

In any case, the magnetic field plays in general a major role in channeling power from the BH (Blandford & Znajek 1977a), or from the disk (Blandford & Payne 1982), into the jet (Maraschi & Tavecchio 2003). In both scenarios, if the magnetic field strength depends, as generally assumed, on the accretion rate (see e.g. Ghisellini et al. 2014), a relation between the accretion rate and the jet power is expected. Various observational studies seem to confirm the link between accretion and ejection (e.g.: Rawlings & Saunders 1991; Celotti et al. 1997; Willott et al. 1999; Maraschi & Tavecchio 2003; Ghisellini 2010; Ghisellini et al. 2014).

In the general picture, FRII radio galaxies host an efficient accretion disk (Shakura & Sunyaev 1973), while FRIs are characterized by hot inefficient accretion flows (ADAF-like; Narayan & Yi 1994; Abramowicz et al. 1995). However, there

is a group of FRII sources that does not fit into this framework. They exhibit powerful extended radio structures but inefficient accretion, attested by their optical spectra typical of LERGs. This kind of objects is not so exotic: indeed, about 25% of sources belonging to the 3CR catalog at $z < 0.3$ and having both radio and optical classifications, are FRII-LERGs (Buttiglione et al. 2009, 2010, 2011).

Therefore, given their peculiar nature and not negligible number, FRII-LERGs constitute a particularly relevant population for the comprehension of the role of the central engine in powering RG jets and in shaping the extended radio morphology.

Within this context, the X-ray band is a fundamental tool to probe the processes at work on different scales from sub-pc up to several hundreds of kpc. To this aim, we performed a systematic and homogeneous X-ray analysis of all FRIIs belonging to the 3CR sample (Bennett 1962) below z<0.3, one of the best studied radio catalogs in all energy bands. For the first time FRII-LERGs are explored as a separate class. Their X-ray and multi-frequency properties are compared to those of FRII-HERGs, in order to understand their nature. For example, they could be FRII-HERGs seen through a thicker obscuring screen or they could have central engines in a "switching-off" phase, in which the standard accretion flow becomes inefficient (ADAF-like). Finally, also the role played by the environment in triggering the AGN and the link between environment and jet power are explored.

This work is organized as follows: in §2 we describe the sample of sources. In §3 we report on the X-ray data reduction and analysis, and discuss our results in §4. In §5 we summarize our conclusions. Throughout the paper we adopt: $H_0 = 71$ km s^{-1} Mpc^{-1}, $\Lambda_\Omega = 0.73$, $\Lambda_m = 0.27$ (Komatsu et al. 2009).
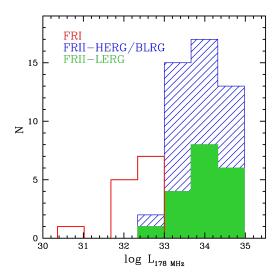
2 THE ANALYZED SAMPLE

The 3CR sources at $z < 0.3$ classified both in the optical (HERGs vs LERGs) and radio bands (FRIs vs FRIIs) are 79. Following Buttiglione et al. (2009, 2010, 2011), who provided the classification in both bands, radio galaxies are divided into:

- 30 FRII-HERGs and 17 FRII-BLRGs[2];
- 19 FRII-LERGs;
- 13 FRIs.

From the radio point of view, the majority of the sources are powerful FRIIs (66), distributed over the entire redshift range, while FRIs (13) represent a small fraction of the total ($\sim 16\%$) and cluster below z<0.05. This is not surprising since low-power RGs are known to be mainly observed at lower redshifts (Laing et al. 1983; Spinrad et al. 1985; Wall & Peacock 1985; Morganti et al. 1993; Burgess & Hunstead 2006a,b). From the optical point of view, the number

---

[1] The excitation index can be defined as:

$EI = log\ [OIII]/H_\beta\ -\ 1/3\ (log\ [NII]/H_\alpha\ +\ log\ [SII]/H_\alpha\ +\ log\ [OI]/H_\alpha)$.

[2] Broad-Lines Radio Galaxies (BLRGs) are classified as HERGs according to their NLR emission. They differ from HERGs for the presence of broad permitted lines in the optical spectrum, coming from the broad line regions (BLR). Therefore, HERGs are classified as type 2 AGN, i.e. edge on, while BLRGs are type 1s, i.e. face on.

Figure 1. Distribution of total radio luminosity at 178 MHz in units of erg s^{-1} Hz^{-1} from Spinrad et al. (1985): FRII-HERGs/BLRGs are in blue, FRII-LERGs are in green and FRIs are in red. While a separation between FRIs and FRIIs is clear, FRII-HERGs/BLRGs and FRII-LERGs completely overlap.

of HERGs/BLRGs (47) and LERGs (32) is not very different, implying that about half of the local radio sources is characterized by a low accretion regime, independently on the radio classification. Indeed, FRII-LERGs and FRII-HERGs/BLRGs span similar values of radio luminosity at 178 MHz, as shown in Figure 1. Following the prescriptions of Willott et al. (1999), if we assume $L_{178 \text{ MHz}}$ as a crude signature of the average jet power over time, FRII-LERGs do not fit in the stardand picture linking powerful jets to efficient accretion flows. Other ingredients have to be considered to explain the observations.

3 X-RAY DATA ANALYSIS

We performed a systematic X-ray analysis of all the FRIIs of the 3CR sample at z<0.3 exploiting archival data from the *Chandra* satellite. This is the most suited telescope to perform such kind of analysis given the good angular resolution ($\approx 0.5''$ in the observational energy band) and the presence of all the sources of the analyzed sample in the public archive [3]. Several of them belong to the 3C *Chandra* legacy survey (Massaro et al. 2010, 2012). However, Massaro et al. adopted a flux sky map method to present the data, while here we follow a different approach based on the direct fit of the data.

We consider FRII-LERGs as key targets of our work (main sample). We also analyze X-ray data of FRII-HERGs/BLRGs as a "control" sample. The goal of our analysis is to investigate the nuclear activity of sources down to the innermost regions (sub-pc scales) both in terms of gas presence (N_{HX}) and X-ray luminosity.

In Table 1 the observation log is reported. All the sources were pointed by *Chandra*.

When more than one observation was available, the data were combined in order to achieve better statistics. We also analyzed all the FRII-LERGs belonging to the XMM-*Newton* archive. In three cases, i.e. 3C 349, 3C 353 and 3C 460, we used XMM-*Newton* data since its larger effective area guaranteed a better constraint of the spectral parameters.

Chandra data were reprocessed using the software CIAO (Chandra Interactive Analysis of Observations), version 4.10 with calibration database CALDB version 4.8.1 and following standard procedures.

A preliminary check of the images was necessary to investigate the presence of extended emission. In case the source was extended, two images were produced: a soft one (0.3-4 keV) and a hard one (4-7 keV). This approach helps in better defining the pointlike emission from the core and modeling its spectrum. Subsequently, VLA radio contours at 1.4 GHz or 5 GHz (with a few arcsec as spatial resolution) were superimposed on the hard X-ray image to properly identify the peak of the nuclear emission and verify the presence of other features such as lobes, jets, knots along the jet. Given the coincidence between the radio core and the X-ray peak in all the analyzed images, no astrometrical correction was applied. The core spectrum was usually extracted from circular regions with a radius ranging between 1.5"-2.5" (depending on the presence or not of extended emission) in order to collect more than 90% of photons. The background was extracted in a clean circular region in the same CCD of the source, avoiding any contamination from field sources or from the source itself.

Spectra were grouped to a minimum of 20 counts per bin in order to adopt the χ^2 statistics. When this was not possible, the C-statistics was applied (Cash 1979) and spectra were grouped to at least one count per bin. For the sources 3C 136.1, 3C 153 and 3C 430 the small number of counts (about 10 counts over the entire spectrum) prevented any modeling. Fluxes and luminosities were estimated using the *Chandra* Proposal Planning Toolkit (PIMMS)[4] and assuming a simple power-law model with $\Gamma = 1.7$ (Grandi et al. 2006). In 3C 196.1, 3C 288, 3C 310 and 3C 388 the AGN emission is completely overwhelmed by the cluster, thus precluding any nuclear study.

XMM-*Newton* data were reduced using the Scientific Analysis Software (SAS) version 16.1 together with the latest calibration files and following standard procedures. Throughout the paper results refer to EPIC/pn data, but all the EPIC instruments were checked.

Source and background spectra were extracted in 0.5-10 keV band from circular regions with radius varying between 20" and 30", depending on the source extension, in order to maximize the S/N ratio. In all cases, at least 80% of photons fell within the extraction region. The background was chosen in a circular region in the same CCD of the source, avoiding any contamination from field sources or from the source itself.

Spectra were grouped to a minimum of 20 counts per bin and the χ^2 statistics was applied.

We checked for the presence of pile-up effects in each source (using the PIMMS software for *Chandra* data and

---

[3] https://cda.harvard.edu/chaser/ .

[4] http://cxc.harvard.edu/toolkit/pimms.jsp .

3CR (1)	Teles. (2)	obsID (3)	date (4)	CCD (5)	t_{exp} (s) (6)
FRII-LERGs - Main sample					
3C88	C	9391	2008-06-30	ACIS-I	11270
	C	11751	2009-10-14	ACIS-S	20180
	C	11977	2009-10-06	ACIS-S	50280
	C	12007	2009-10-15	ACIS-S	35080
3C132	C	9329	2008-03-26	ACIS-S	7790
3C153	C	9302	2007-12-07	ACIS-S	8170
3C165	C	9303	2008-02-02	ACIS-S	7770
3C166	C	12727	2010-11-29	ACIS-S	8050
3C173.1	C	3053	2002-11-06	ACIS-S	24310
3C196.1	C	12729	2011-02-11	ACIS-S	8050
3C213.1	C	9307	2008-04-14	ACIS-S	8170
3C236	C	10249	2009-01-14	ACIS-I	41040
3C288	C	9275	2008-04-13	ACIS-S	40150
3C310	C	11845	2010-04-09	ACIS-S	58320
3C326	C	10908	2009-05-10	ACIS-I	27880
3C349	X	0501620301	2007-08-07	EPIC/pn	14863
	X	0501621601	2007-10-03	EPIC/pn	15113
3C353	X	0400930101	2006-08-25	EPIC/pn	44264
	X	0400930201	2007-02-17	EPIC/pn	10916
3C357	C	12738	2010-10-31	ACIS-S	8050
3C388	C	5295	2004-01-29	ACIS-I	31120
3C401	C	4370	2002-09-21	ACIS-S	25170
	C	3083	2002-09-20	ACIS-S	22960
3C430	C	12744	2011-11-14	ACIS-S	8050
3C460	X	0675400101	2011-12-24	EPIC/pn	48744
FRII-HERGs/BLRGs - Control sample					
3C20	C	9294	2007-12-31	ACIS-S	8040
3C33	C	7200	2005-11-12	ACIS-S	20180
3C61.1	C	9297	2008-12-05	ACIS-S	8160
3C79	C	12723	2010-11-01	ACIS-S	7790
3C98	C	10234	2008-12-24	ACIS-I	32130
3C105	C	9299	2007-12-17	ACIS-S	8180
3C133	C	9300	2008-04-07	ACIS-S	8140
3C135	C	9301	2008-01-10	ACIS-S	8040
3C136.1	C	9326	2008-01-10	ACIS-S	10040
3C171	C	10303	2009-01-08	ACIS-S	60220
	C	9304	2007-12-22	ACIS-S	8040
3C180	C	12728	2010-12-24	ACIS-S	8060
3C184.1	C	9305	2008-03-27	ACIS-S	8130
3C192	C	9270	2007-12-18	ACIS-S	10150
	C	19496	2017-12-18	ACIS-S	70110
	C	20888	2017-12-21	ACIS-S	10070
	C	20889	2017-12-21	ACIS-S	33110
	C	20890	2017-12-24	ACIS-S	21410
	C	20891	2017-12-22	ACIS-S	35760
3C223	C	12731	2012-01-07	ACIS-S	8050
3C223.1	C	9308	2008-01-16	ACIS-S	8030
3C234	C	12732	2011-01-19	ACIS-S	8050
3C277.3	C	11391	2010-03-03	ACIS-S	25120
	C	15023	2014-03-15	ACIS-I	44080
	C	15024	2014-03-16	ACIS-I	20090
	C	16600	2014-03-11	ACIS-I	98080
	C	16599	2014-03-13	ACIS-I	29090
3C284	C	12735	2010-11-17	ACIS-S	8050
3C285	C	6911	2006-03-18	ACIS-S	40150
3C300	C	9311	2008-03-21	ACIS-S	8040
3C303.1	C	9312	2008-02-21	ACIS-S	7770
3C305	C	9330	2008-04-07	ACIS-S	8330
	C	12797	2011-01-03	ACIS-S	29040
	C	13211	2011-01-06	ACIS-S	29040
3C321	C	3138	2002-04-30	ACIS-S	47730
3C327	C	6841	2006-04-26	ACIS-S	40180
3C379.1	C	12739	2011-04-04	ACIS-S	8050
3C381	C	9317	2008-02-21	ACIS-S	8170
3C403	C	2968	2002-12-07	ACIS-S	50130
3C436	C	9318	2008-01-08	ACIS-S	8140
	C	12745	2011-05-27	ACIS-S	8060
3C452	C	2195	2001-08-21	ACIS-S	80950
3C456	C	12746	2011-01-17	ACIS-S	8050
3C458	C	12747	2010-10-10	ACIS-S	8050
3C459	C	12734	2011-10-13	ACIS-S	8050
	C	16044	2014-10-12	ACIS-S	59960

Table 1. Observation log of FRII-LERGs (main sample) and FRII-HERGs/BLRGs (control sample). Column description: (1) 3CR name; (2) Telescope: C=*Chandra* and X=XMM-*Newton*; (3) Observation ID; (4) Start date of the observation; (5) Instrument used in the observation; (6) Total exposure time in seconds. All the sources are the target of the observation.

the task EPATPLOT in the SAS for *XMM-Newton* data). The pile-up was generally negligible ($< 10\%$) or absent in FRII-LERGs, but turned out to be important in FRII-HERGs/BLRGs seen face-on (i.e. BLRGs). Indeed, we could perform a *Chandra* spectral analysis only for two BLRGs, i.e. 3C 184.1 and 3C 459, for which the estimated pile-up was less than $< 10\%$.

The spectral analysis was performed using the XSPEC version 12.9.1 (Arnaud 1996). The energy range considered in the spectral fitting was 0.3-7 keV for *Chandra* and 0.5-10 keV for XMM-*Newton*. Errors reported are quoted at 90% confidence for one parameter of interest (Avni 1976).

3.1   Spectral analysis

An ispection of the X-ray images indicate that 6 out of 19 FRII-LERGs show strong emission over the galaxy-scale (from several tens to hundreds of kpc) due to hot gas from cluster (Figure 2). On the contrary, no FRII-HERGs/BLRGs show cluster emission in the *Chandra* images, although some of them show resolved emission on kpc-scale.

At first, we considered as baseline model a single power-law convolved with Galactic column density (Kalberla et al. (2005); PHABS). When the power-law spectral slope was less than 1 an intrinsic absorption component (ZPHABS) was added to the fit. Because of the poor statistics and/or the complexity of the emission, we were forced to fix the hard photon index ($\Gamma = 1.7$) in 7 out of 19 FRII-LERGs and in 27 out of 32 FRII-HERGs/BLRGs (see Table 2). If no XMM-*Newton/Chandra* information on the power-law spectral slope was available in literature, we chose a reliable value of $\Gamma = 1.7$. Nonetheless, we checked whether different values of the photon indices could produce significant changes in the estimate of the column density. However, even assuming different photon indices ($\Gamma = 1.4$ and $\Gamma = 2.0$), the column densities and the intrinsic luminosity remain consistent within the errors[5]. If residuals were still present at soft-energies a second power-law, or a thermal emission (MEKAL) were added to the fit. A second power-law is expected if the primary component is scattered by clouds of electrons above the torus. A thermal emission is expected if the source is embedded in a gaseous environment, i.e. hot corona of early-type galaxies (Fabbiano et al. 1992) or intergalactic medium. The MEKAL model could also roughly mimic features related to photoionized gas, given the limited energy resolution of CCD detectors. Therefore, after testing for collisional gas presence, if prominent photoionized features were present in the soft X-ray spectrum yet, a fit with multiple narrow emission lines (Gaussian-profile) was tested.

In the hard spectrum, a Gaussian component (ZGAUSS) was included if positive residuals were observed in the region of the iron Kα line (5-7 keV). Once the Fe kα line was

---

[5] For all the sources with fixed spectral slope, the N_H and L_X values do not change respectively more than $\approx$15% and 40% varying the power law spectral slope from 1.4 to 2.0. As the uncertainties of the same quantities in Table 2 are above 70%, we are confident that the $\Gamma = 1.7$ assumption does not significantly affect our results.

attested, the presence of a reflection component (PEXRAV) was verified: in fact, this is expected when cold matter surrounding the nuclear engine reprocesses the primary X-ray radiation (Lightman & White 1988). In this case, the cutoff energy and the angle between the normal to the disk and the observer were fixed to 100 keV and 30°, respectively. The reflection component is modeled by the parameter $R = \Omega/2\pi$, corresponding to the solid angle fraction of a neutral, plane parallel slab illuminated by the continuum power-law (PEXRAV). Given the low statistics and the limited energy range covered by *Chandra* and *XMM-Newton*, small variations in these parameters do not impact the fit.

3.2 Results

The results of the X-ray analysis, listed in Table 2, are in substantial agreement with those reported in the literature using different satellites and/or different approaches (e.g. Grandi et al. 2006; Evans et al. 2006; Massaro et al. 2010, 2012). Details on the soft X-ray component and reprocessed features are listed in Tables 3 and 4, respectively.

The photon index of FRII-LERGs was tightly constrained for 8 out of 19 sources: the mean Γ value is 1.7 and the standard deviation is 0.3 (see Table 2). Intrinsic cold gas obscuration was required in about 50% of the sources. They are generally moderately absorbed, with a N_{HX} of the order of a few 10^{22} cm^{-2}. Only in two radio galaxies, i.e. 3C 173.1 and 3C 460, the column density reaches values of few 10^{23} cm^{-2}. An iron Kα line was detected in 3C 353 (see Table 4) with an intensity, within the large uncertainties, compatible with being produced by the same matter obscuring the nuclear region (Ghisellini et al. 1994). For the other objects with intrinsic absorption, the feature could not be revealed because of the low statistics and the abrupt drop of the *Chandra* effective area above 6-7 keV.
When present, the soft X-ray excess is well described by a power-law, that is probably scattered nuclear emission. Indeed, the normalization values of the scattered component at 1 keV are always a few percent of the absorbed one: the mean value is 6%, in agreement with those measured for type 2 Seyferts (e.g. Bianchi & Guainazzi 2007).
The cluster emission, when present in the X-ray images, is generally dominant. In four cases (3C 196.1, 3C 288, 3C 310, 3C 388), the AGN is overwhelmed by the thermal gas and any nuclear study is precluded. Therefore, for these sources the estimated 2-10 keV luminosity should be considered as an upper limit of the nuclear AGN emission. Only in 3C 88, the AGN spectrum was disentangled from the thermal emission and it is analogous to that of the other absorbed radio galaxies. Instead, in 3C 401 the AGN emission dominates over the cluster one and the nuclear spectrum is well reproduced by a single power-law. The intrinsic absorption is negligible, and indeed only an upper limit is provided (see Table 2).

The spectra of the control sample (FRII-HERGs/BLRGs) are generally more complex than FRII-LERGs (see Table 2). About 90% of them show strong obscuration, with typical values one order of magnitude higher than FRII-LERGs ($N_H \sim 10^{23}$ cm^{-2}). The photon index could be well con-

strained in only 15% (5 out of 32) of sources ($< \Gamma > = 1.8$ and $\sigma_{rms} = 0.5$). Intense iron lines with Equivalent Width (EW) spanning from 140 eV to more than 1 keV are detected in 11 sources and, in at least two cases, a Compton reflection model was also required (Table 4). These reprocessed features, signature of a complex and inhomogeneous circumnuclear absorber, are commonly observed in Seyfert-like spectra (Risaliti 2002).

The soft X-ray excess of >50% of FRII-HERGs/BLRGs is generally well reproduced by a second power-law, which can be interpreted as the scattered component of the primary one. The mean unabsorbed normalization at 1 keV is 8% of the absorbed one. In addition to the second power-law, a MEKAL model is required in a few objects: in some cases, this component is directly related to collisional gas emission (cluster or shocked gas), in the other ones it could mimic photoionized features (Balmaverde et al. 2012). Indeed, in two radio galaxies, i.e. 3C 403 and 3C 321, single soft X-ray emission lines associated to Ne IX, O VII and Mg XI were revealed in the spectrum.

In summary, the control sample show more complex and feature-rich spectra than the key sample. FRII-HERGs/BLRGs are characterized by mean values of intrinsic absorption and X-ray luminosity one order of magnitude larger than FRII-LERGs, implying a substantially higher activity of the central engine and more variegated circumnuclear environment.

4 DISCUSSION

The aim of the present study is to explore the jet-accretion connection and the role of the environment in shaping the radio morphology in sources of different FR type. Our X-ray results can be summarized as follows:

• nearly 30% of FRII-LERGs are in a dense/extended gaseous environment, as attested by the *Chandra* images. Thermal gas is also detected in several images of the FRII-HERGs/BLRGs control sample. The extension of the emission seems to suggest a galactic rather than an intergalactic origin;
• FRII-LERGs' spectra are generally well modeled by a power-law absorbed by a moderate intrinsic column density ($N_H \sim 10^{22}$ cm^{-2}). Conversely, FRII-HERGs/BLRGs have spectra rich in features and engines obscured by high column densities ($N_H \geq 10^{23}$ cm^{-2});
• FRII-LERGs are intrinsically less luminous than FRII-HERGs/BLRGs by a factor of ten in the 2−10 keV band.

4.1 Are FRII-LERGs obscured FRII-HERGs/BLRGs?

The first scenario that we explore supposes that FRII-LERGs could be obscured FRII-HERGs/BLRGs.
Our analysis does not support this hyphotesis. The gas column densities, estimated from the X-ray spectra, carry out information on the environment down to sub-parsec scales. Looking at Table 2, the difference between the FRII classes in terms of N_H is evident: FRII-HERGs/BLRGs are more obscured than FRII-LERGs. A two-sample test univariate
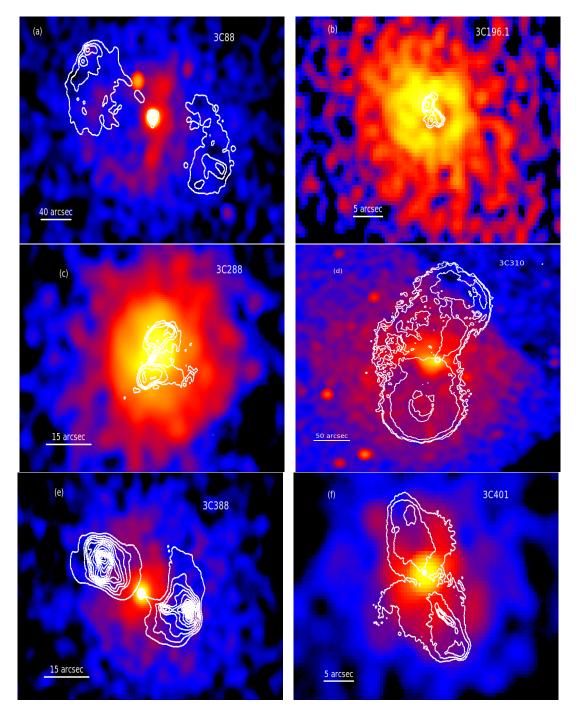
Figure 2. *Chandra* 0.3-7 keV images of extended FRII-LERGs. Radio VLA contours at 5 GHz and 1.4 GHz (*white*) are superimposed to the X-ray images. Panel (a): **3C 88** inhabits the center of a galaxy group and produce the largest X-ray cavities ever found in such an environment (Liu et al. 2019). Panel (b): **3C 196.1** is the Brightest Cluster Galaxy (BCG) of a Cool Core Cluster (CCC). Ricci et al. (2018) measured a core cluster temperature kT~ 3 keV, in agreement with our analysis (see Table 3). Panel (c): **3C 288** resides the center of a poor not-CC cluster, as shown by Lal et al. (2010). They found an ICM gas temperature kT~3 keV extending up to 400 kpc. Panel (d): **3C 310** is the central galaxy of a poor cluster with a temperature of about 3 keV at a distance between 100 and 180 kpc (at which a shock occurs) (Kraft et al. 2012). Panel (e): **3C 388** resides in the center of a small cluster environment with an ICM temperature of about 3.5 keV and a cool core probably heated by a nuclear outburst (Kraft et al. 2006). Panel (f): **3C 401** is in the center of a cluster with ICM mean temperature of 2.9 keV. Reynolds et al. (2005) proposed both a thermal hot core ($T \approx 4.9$ keV) and a simple power law model (which is the model assumed in this work) because statistically indistinguishable.

Table 2. Spectral parameters of the X-ray continuum.

Name	z	$N_{H,Gal}$ $(10^{20}$ cm$^{-2})$	Fitted Model[a]	$N_{H,intr}$ $(10^{22}$ cm$^{-2})$	Γ_H	$L_{2-10\ keV}$ $(10^{42}$ erg s$^{-1})$	Statistics[b]
			FRII-LERGs				
3C 88	0.0302	8.3	[iii]	2.0 ± 0.5	1.6 ± 0.3	0.4 ± 0.2	36.9/50
3C 132	0.214	21.3	[ii]	5^{+4}_{-3}	$1.7^\dagger$	22^{+12}_{-8}	4.1/5 C
3C 153*	0.2769	16.2	[i]	-	$1.7^\dagger$	< 1.5	-
3C 165	0.2957	19.4	[ii]	3 ± 2	$1.7^\dagger$	23^{+11}_{-8}	8.2/14 C
3C 166	0.2449	17.1	[i]	< 0.16	1.6 ± 0.2	80 ± 10	20.1/19
3C 173.1	0.292	4.5	[vi]	30^{+200}_{-20}	$1.7^\dagger$	27^{+180}_{-16}	35.3/25 C
3C 196.1	0.198	6.0	[vii]	-	-	< 9.6	20.5/13 C
3C 213.1	0.1939	2.4	[i]	< 0.43	$1.9^{+0.5}_{-0.4}$	4 ± 1	15.4/9 C
3C 236	0.1005	1.0	[ii]	$1.9^{+0.6}_{-0.5}$	1.4 ± 0.3	12^{+7}_{-4}	27.0/29
3C 288	0.246	0.8	[vii]	-	-	< 4.7	6.4/6
3C 310	0.0535	3.7	[vii]	-	-	< 0.02	10.5/17 C
3C 326	0.0895	9.0	[ii]	$2.2^{+2.8}_{-1.7}$	$1.7^\dagger$	$0.2^{+0.2}_{-0.1}$	3.4/3 C
3C 349	0.205	1.9	[ii]	0.9 ± 0.2	1.4 ± 0.2	60 ± 10	46.2/47
3C 353	0.0304	9.3	[vi]	$6.7^{+0.9}_{-0.8}$	1.7 ± 0.2	3 ± 1	58.0/61
3C 357	0.1662	3.1	[iii]	3 ± 2	2 ± 1	22^{+6}_{-12}	17/18 C
3C 388	0.0917	5.5	[vii]	-	-	< 0.9	62.5/59 C
3C 401	0.2011	5.9	[i]	< 0.16	1.7 ± 0.1	5.0 ± 0.5	15.9/18
3C 430*	0.0541	33.1	[i]	-	$1.7^\dagger$	< 0.05	-
3C 460	0.268	4.72	[iii]	25^{+23}_{-11}	$1.7^\dagger$	20 ± 10	5.7/6
			FRII-HERGs/BLRGs				
3C 20	0.174	18.0	[ii]	15^{+4}_{-3}	$1.7^\dagger$	110^{+30}_{-20}	24.1/25 C
3C 33	0.0596	3.4	[v]	53^{+8}_{-7}	$1.7^\dagger$	100^{+30}_{-20}	32.5/40
3C 61.1	0.184	7.9	[iii]	29^{+23}_{-12}	$1.7^\dagger$	40^{+40}_{-20}	30/18 C
3C 79	0.2559	8.7	[iii]	33^{+12}_{-10}	$1.7^\dagger$	270^{+130}_{-90}	14.4/16 C
3C 98	0.0304	10.0	[iv]	$9.4^{+1.0}_{-0.9}$	$1.7^\dagger$	$5.3^{+0.5}_{-0.3}$	57.4/48
3C 105	0.089	12.0	[iv]	43^{+7}_{-6}	$1.7^\dagger$	220^{+90}_{-50}	13.6/12
3C 133	0.2775	25.0	[ii]	$0.8^{+0.4}_{-0.3}$	2.0 ± 0.3	190^{+80}_{-50}	39.4/26
3C 135	0.1253	8.7	[vi]	34^{+32}_{-19}	$1.7^\dagger$	14^{+23}_{-8}	15.8/13 C
3C 136.1*	0.064	32.0	[i]	-	$1.7^\dagger$	< 0.06	-
3C 171	0.2384	5.7	[ii]	7 ± 1	1.5 ± 0.3	130^{+80}_{-50}	33.8/26
3C 180	0.22	14.0	[iii]	70^{+160}_{-50}	$1.7^\dagger$	90^{+1800}_{-70}	7.1/7 C
3C 184.1	0.1182	3.2	[iii]	8 ± 1	$1.7^\dagger$	110 ± 10	19.8/24
3C 192	0.0598	3.9	[iii]	34^{+8}_{-7}	1.7 ± 0.5	2^{+4}_{-1}	14.3/18
3C 223	0.1368	1.0	[iii]	13^{+13}_{-7}	$1.7^\dagger$	20^{+16}_{-8}	10/10 C
3C 223.1	0.107	1.3	[ii]	28 ± 6	$1.7^\dagger$	90^{+30}_{-20}	9.3/12 C
3C 234	0.1848	1.8	[vi]	17^{+9}_{-6}	$1.7^\dagger$	150^{+70}_{-50}	6.6/8
3C 277.3	0.0857	0.9	[xiii]	27^{+6}_{-5}	$1.7^\dagger$	9^{+2}_{-1}	23.1/21
3C 284	0.2394	0.9	[i]	< 0.91	2.3 ± 1.0	$1.1^{+0.4}_{-0.5}$	1.4/5 C
3C 285	0.0794	1.3	[vi]	38^{+8}_{-6}	$1.7^\dagger$	35^{+10}_{-7}	7.7/11
3C 300	0.27	2.5	[i]	< 0.19	1.4 ± 0.3	13 ± 2	12.7/10 C
3C 303.1	0.267	3.0	[ii]	18^{+132}_{-16}	$1.7^\dagger$	15^{+400}_{-11}	0.1/2 C
3C 305	0.0416	1.3	[viii]	< 0.72	$1.7^\dagger$	0.04 ± 0.01	36.3/24 C
3C 321	0.096	3.8	[ix]	26^{+20}_{-13}	$1.7^\dagger$	4^{+4}_{-2}	61.2/40 C
3C 327	0.1041	5.9	[x]	30^{+63}_{-18}	$1.7^\dagger$	8^{+31}_{-4}	46.6/25
3C 379.1	0.256	5.4	[vi]	60^{+70}_{-30}	$1.7^\dagger$	110^{+400}_{-70}	7.3/8 C
3C 381	0.1605	9.9	[iii]	30^{+7}_{-6}	$1.7^\dagger$	240^{+70}_{-50}	18.9/21 C
3C 403	0.059	12.1	[xi]	46 ± 3	$1.7^\dagger$	78^{+10}_{-9}	51.5/57
3C 436	0.2145	6.7	[iii]	48^{+22}_{-15}	$1.7^\dagger$	100^{+80}_{-40}	14.4/15 C
3C 452	0.0811	9.8	[v]	53^{+8}_{-7}	$1.7^\dagger$	100 ± 20	77.9/78
3C 456	0.233	3.7	[ii]	7 ± 1	$1.7^\dagger$	160 ± 20	63.6/59 C
3C 458	0.289	5.9	[ii]	35^{+20}_{-16}	$1.7^\dagger$	150^{+140}_{-70}	16.8/14 C
3C 459	0.2199	5.2	[xii]	4^{+3}_{-2}	$1.7^\dagger$	12^{+3}_{-2}	31.2/25

[a] – All the adopted models are absorbed by the Galactic column density:[i] po;[ii] zpha*po;[iii] zphabs*po+po; [iv] zphabs*(po+zgauss)

[v] zphabs*(po+zgauss)+po+pexrav); [vi] zphabs*(po+zgauss)+po;[vii] mekal;[viii] mekal+po;[ix] zphabs*(po+zgauss)+po+2zgauss;

[x] zphabs*(po+zgauss)+po+ mekal;[xi] zphabs*(po +zgauss)+po+2zgauss+mekal; [xii] zphabs*(po)+po+mekal; [xiii] zphabs*(po+zgauss)+zphabs*po

[b] – Statistics refers to the entire energy band assuming the model listed in column (4). "C" indicates that the C-statistics was adopted.

† – fixed photon index

* – luminosities estimated with PIMMS assuming a simple power law model with $\Gamma = 1.7$.

program, TWOST (Feigelson & Nelson 1985; Isobe et al. 1986), that takes into account upper limits, confirms that the two samples are different, being $P_{TWOST} = 7 \times 10^{-4}$. We assume $P_{TWOST} = 0.05$ as the probability threshold to rule out the hypothesis that two samples are drawn from the same population.

To take a step forward, 3CR/FRI radio galaxies with X-ray information available from literature (Balmaverde et al. 2006) were also compared to the FRII samples. The peak of the N_H distribution in FRIs is clearly shifted to lower values, as shown in Figure 3. There is a partial overlap with FRII-LERGs. However, a TWOST test applied to FRII-LERGs and FRIs provides a probability of $P_{TWOST} = 2 \times 10^{-2}$, showing that these two samples are intrinsically different. Instead, the same test confirms that FRII-HERGs/BLRGs and FRIs are drawn from different populations ($P_{TWOST} < 10^{-4}$). It is interesting to note that larger amounts of cold gas column densities are associated to radio galaxies with efficient accretion disks.

We conclude that there is an indication that the quantity of obscuring matter (in the form of cold gas) is decreasing from FRII-HERGs/BLRGs to FRIs, with FRII-LERGs lying in between.

Another source of obscuration is the dust spread in the galaxy, that could affect our optical measurements. Note that the optical classification of radio galaxies provided by Buttiglione et al. (2009) is based on lines produced in the NLR.

The dust content can be estimated using the Balmer decrement. Adopting an extinction curve $\kappa(\lambda)$, the intrinsic color excess can be expressed as:

$$E(B-V)_i = \frac{2.5}{[\kappa(H_\beta) - \kappa(H_\alpha)]} \times \log\left[\frac{(H_\alpha/H_\beta)_o}{3.1}\right]$$

.

Details on the derivation of the above formula can be found in the Appendix of Momcheva et al. (2013). The theoretical (H_α/H_β) ratio is 2.86, as expected if the temperature and the electron density of the NLR are $T = 10^4$ K and $N_e = 10^3$ cm^{-3}, respectively (Osterbrock 1989). Actually, a value of 3.1 is considered the best prescription for AGN (Gaskell 1982, 1984; Wysota & Gaskell 1988; Tsvetanov & Iankulova 1989; Heard & Gaskell 2016). Several functional forms for the attenuation curve are present in literature. The most used are: the Milky Way extinction curve (Cardelli et al. 1989), the Large and Small Magellanic Cloud extinction curves from Gordon et al. (2003) and a general extra-galactic extinction curve from Calzetti (1997). The reddening study was performed considering all the different extinction curves. As the results are similar, hereafter the discussion is based on the Milky Way extinction curve.

Buttiglione et al. (2010) provided the narrow H_α and H_β fluxes for the majority of 3C radio galaxies up to $z=0.3$. We could then investigate the amount of dust in FRIs, FRII-LERGs and FRII-HERGs/BLRGs by simply comparing the $(H_\alpha/H_\beta)_o$ ratio (assuming the same extinction curves for all the galaxies). In Figure 4, a histogram of the Balmer decrement for all the sources with detected lines (74 out of 79) is presented. When the flux ratio was less than the theoretical value, the source was considered unabsorbed (i.e. $(H_\alpha/H_\beta)_o = 3.1$). It is immediate to note that the FRIs'
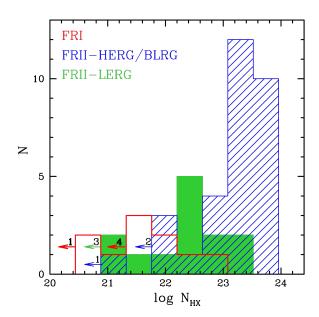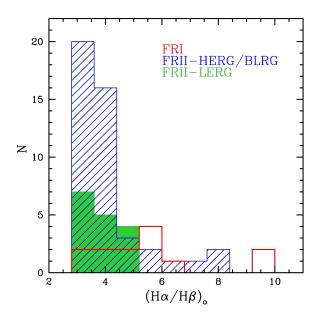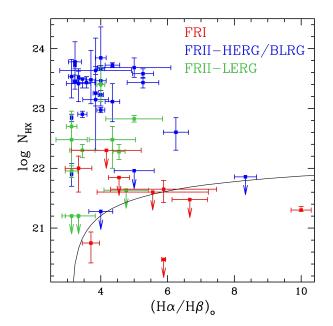

Figure 3. Distribution of the intrinsic gas column density N_{HX} in units of cm^{-2}, as measured in the X-ray band. The FRII-LERGs population (*green*) is on average less obscured than FRII-HERGs/BLRGs (*blue*), but more than FRIs (*red*). Arrows indicate upper limits with the number of sources per bin specified. FRIs data are taken from Balmaverde et al. (2006).

Figure 4. Distribution of the observed Balmer decrement $(H_\alpha/H_\beta)_o$ used to estimate the dust extinction for the three classes of radio galaxies considered in this work, i.e. FRII-LERGs, FRII-HERGs/BLRGs and FRIs. H_α and H_β flux measurements are taken from Buttiglione et al. (2009). We assume the theoretical $(H_\alpha/H_\beta)_o=3.1$ as a reliable value for AGN (see Section 4.1). When $(H_\alpha/H_\beta)_o < 3.1$, the source is considered unabsorbed.

Figure 5. Column density (N_{HX}), as obtained by the X-ray analysis, plotted versus the intrinsic reddening, as measured by the optical Balmer decrement $(H\alpha/H\beta)_o$. N_{HX} decreases from FRII-HERGs/BLRGs to FRI. FRII-LERGs occupy the middle region of the plot. FRIs show the highest excess of colour and the lowest gas content. The black curve represents the expected N_H value assuming a dust-to-gas ratio $N_H/E(B-V)=5.8\times10^{21}$ atoms cm^{-2} mag^{-1}.

distribution peaks to higher values of $(H_\alpha/H_\beta)_o$. Indeed, a Kolmogorov-Smirnov (KS) test confirms that FRIs are richer in dust than both FRII-LERGs ($P_{KS} = 0.01$) and FRII-HERGs/BLRGs ($P_{KS} = 0.008$). The current optical data do not allow us to exclude that the two FRII classes are drawn from the same population ($P_{KS} = 0.32$).

Therefore, the difference between FRII-LERGs and FRII-HERGs/BLRGs is intrinsic and not an artefact due to different absorbing screens.

In Figure 5 the column density (N_{HX}) measured in the X-ray band is plotted vs $(H_\alpha/H_\beta)_o$. This plot traces the obscuring matter at different scales: N_{HX} maps the gas down to sub-pc scales, while the optical lines $(H_\alpha/H_\beta)_o$ (i.e., E(B-V)), carries out information from the NLR.

Different classes appear to populate distinct regions of the plot: FRII-HERGs/BLRGs, having higher N_{HX} values, mainly cluster in the upper part of the plot, FRII-LERGs occupy a similar region but are shifted to lower N_{HX}, FRIs lie at the bottom of N_{HX} but extend to $(H_\alpha/H_\beta)_o$ up to 10. Moreover, all FRIs are at the edge or below the N_H line that traces the expected amount of gas according to a standard Galactic gas to dust ratio $N_H=5.8 \times 10^{21}$ E(B-V) atoms cm^{-2} mag^{-1} (Bohlin et al. 1978). Conversely, all the FRIIs are above the N_H line, suggesting a large amount of gas (although with different column densities) near the BH and paucity of dust in the NLR and/or along the galaxy.

The dichotomy between FRII-LERGs and FRII-HERGs/BLRGs is reinforced by the X-ray analysis. The unabsorbed X-ray luminosity divided by the Eddington luminosity ($L_{Edd}=1.3\times10^{38}$ M/M$_\odot$ erg s^{-1}) is a direct proxy

of the accretion rate ($L_{2-10\ keV}/L_{Edd}$; Merloni et al. 2003). The BH masses for the sources in our sample were calculated by exploiting the relation between the H-band host-galaxy magnitude (taken from Buttiglione et al. 2009) and M_{BH}, provided by Marconi & Hunt (2003) (with a dispersion of ~ 0.3 dex in the BH mass). As expected, no significant difference in masses is observed among FRIs and FRIIs. The M_{BH} range is narrow: $10^{8.5} - 10^{9.5}$ M$_\odot$.
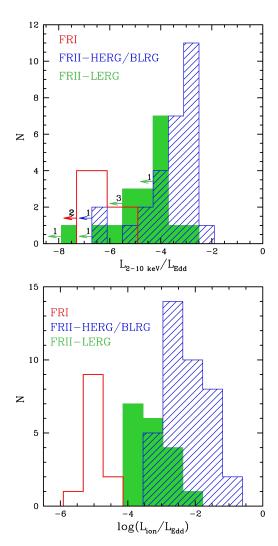
The upper panel of Figure 6 shows the $L_{2-10\ keV}/L_{Edd}$ distribution for the three classes. The distributions of FRIs and FRII-HERGs/BLRGs are clearly separated ($P_{TWOST} < 10^{-4}$), while FRII-LERGs are in between. The displacement of FRII-LERGs' peak towards lower accretion rates is confirmed by a TWOST test, that associates a probability of 10^{-4} and 5.8×10^{-3} to the hypothesis that FRII-LERGs are drawn from the same parent population of FRII-HERGs/BLRGs and FRIs, respectively. *Therefore, the nuclear activity is inherently different in FRIs, FRII-LERGs and FRII-HERGs/BLRGs.*

Note that for RGs with ADAF-like engine the estimated X-ray luminosity could provide an upper limit of the accretion luminosity, as there could be a significant contribution from the jet emission. If this were the case, the separation between FRII-LERGS and FRII-HERGs/BLRGs would be even more pronounced. Finally, we note that the same trend is observed when the ionizing radiation L_{ion} in terms of the Eddington luminosity is considered (lower panel of Figure 6). This quantity, defined as Log L_{ion} ~ Log $L_{[OIII]}$ + 2.83 (Buttiglione et al. 2009) is directly related to the accretion efficiency, being responsible for the excitation of the NLR gas.

The agreeement between upper and lower panels of Figure 6 corroborates our previous conclusion based on the $(H_\alpha/H_\beta)_o$ study. As no dust correction was applyed to L_{ion}, the different optical classification of FRIIs **cannot** be ascribed to optical NLR obscuration.

4.2 Were FRII-LERGs powerful FRII-HERGs/BLRGs in the past?

The comparison of the X-ray and $L_{[OIII]}$ luminosities, accretion rates, and intrinsic nuclear absorption among the examined classes of sources have solidly established that FRII-LERGs have intermediate properties, lying between FRIs and FRII-HERGs/BLRGs. It is plausible that FRII-LERGs represent an evolutionary stage of FRII-HERGs/BLRGs. A link between the accretion properties and the power of the produced jets is certainly expected, based on both theoretical arguments (e.g., Blandford & Znajek 1977b; Sikora et al. 2007) and observational works (e.g., Allen et al. 2006; Ghisellini et al. 2014). Since the FRII-LERGs in this sample accrete at lower rates than classic FRII-HERGs/BLRGs, we would then expect their jets to be correspondingly less powerful. Contrarily to this expectations, their extended radio luminosities, generally assumed as predictors of the total jet power (e.g., Cavagnolo et al. 2010a), are very similar (see Figure 1). This conflict can be bypassed considering the large-scale radio structures of FRII-LERGs as the heritage of a past AGN activity at higher efficiency. If the nuclear activity has recently decreased due, for instance, to the depletion of the cold gas reservoir, it is reasonable to think that this information may not have reached the large-scale

Figure 6. *Upper panel:* X-ray luminosity normalized for the Eddington luminosity. FRIs are in red, FRII-LERGs are in green and FRII-HERGs/BLRGs are in blue. Leftwards arrows indicate upper limits, with specified number per bin and population. *Lower panel:* estimated L_{ion}/L_{Edd} ratio. Both accretion rate estimates show the same trend: FRIs at the lowest values, classical FRIIs at the highest ones, and FRII-LERGs in between.

radio structures yet, which are formed at kilo-parsec distances from the central engine.

The evolutionary scenario is also supported by a recent analysis of a large sample of low-redshift and low-luminosity FRIIs objects (Capetti et al. 2017), which showed that the roughly one-to-one correspondence between FRII morphologies and powerful nuclei is not verified for this large population in the local universe (z<0.15). On the contrary, most of the FRIIs in the catalog compiled by Capetti et al. (2017) are classified as LERGs. This could suggest that the local FRIIs are "starved", i.e. they now miss the fueling cold material that made them shine in the past.
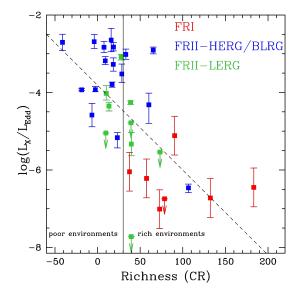
4.3   Does the environment play a role?

Another possibility is that the nuclei of FRII-LERGs, while not as powerful as in classic FRII-HERGs/BLRGs, can still

form FRII morphologies due, for instance, to favorable environmental conditions. Several studies in literature identify the environment as the fundamental ingredient for the origin of the FRI/FRII dichotomy. Gendre et al. (2013), studying the cluster richness for a large sample of radio galaxies, suggest that the relation between radio morphology and accretion mode is quite complex and attribute to the environment an important role. They calculated the cluster richness (CR) following the method of Wing & Blanton (2011), that is based on the count of galaxies within a disk of 1 Mpc of radius around each analyzed target. Then, they concluded that FRII-HERGs/BLRGs and FRIs live in different ambients, being characterized by poor and rich environments, respectively. On the contrary, they found that the 29 FRII-LERGs of their sample can live both in clusters ($\approx 40\%$) and in scarcely populated regions (in terms of richness, $\approx 60\%$).

Our X-ray data confirm that FRII-LERGs can actually be set in a dense and hot medium Indeed, 6 out of 19 are found in clusters (see Figure 2).. Unfortunately, our X-ray analysis, exploiting data from public archives, suffers from an inhomogeneity of the exposure times that prevents a comparative study on the environments among the different classes. Taking advantage of the richness study of Gendre et al. (2013), we could explore the relation between accretion, in terms of $L_{2-10\ keV}/L_{Edd}$, radio morphology and environment for 18 FRII-HERGs/BLRGs, 8 FRIs and 9 FRII-LERGs. In Figure 7 the X-ray luminosity scaled for the Eddington luminosity is plotted as a function of CR for the three classes. The vertical line is the limit between poor (CR<30) and rich (CR>30) environments proposed by Gendre et al. (2013). As expected, FRII-HERGs/BLRGs occupy the left upper corner (i.e. they are in less dense environments and have more efficient engines), while FRIs are segregated in the right lower region (i.e. they have high CR and low $L_{2-10\ keV}/L_{Edd}$ values). The intermediate accretion rates of FRII-LERGs put them in the middle part of the diagram, but, unlike the other classes, they fall into both sides of the threshold fixed at CR=30. More impressive is the clear link in the whole sample between the richness of the environment and the accretion in terms of $L_{2-10\ keV}/L_{Edd}$. A Kendall$-\tau$ test in ASURV provides a very high probability that these quantities are correlated ($P_{Kendall-\tau} > 99.9\%$). With the appropriate caution required by the limited number of sources, this result suggests that the environment would have a strong impact on the accretion regime.
The problem with this interpretation is that the radio luminosity of the extended components, related to the jet kinetic power, is similar in FRIIs, at odds with what is observed in X-rays, where FRII-HERGs/BLRGs are brighter (more efficient accretors) than FRII-LERGs.
However, the relation $P_{jet} \propto L_{151\ MHz}^{6/7}$, proposed by Willott et al. (1999) and widely used in literature, is calibrated on FRII radio galaxies and suffers from large uncertainties represented by a factor $f^{3/2}$, that mainly depends on the ratio between the energy in protons and eletrons in the lobes. Willott et al. (1999) deduced that f can span from 1 to 20, implying a P_{jet} uncertainty of about two orders of magnitude. Other authors revisited this relation measuring the jet power using the X-ray cavities produced by the interaction of FRI jets (Bîrzan et al. 2008; Cavagnolo et al. 2010b) or the hot-spot size and an equipartition magnetic field in

Figure 7. Environmental richness (CR) plotted versus the intrinsic Eddington-scaled X-ray luminosity. Color-coding is the same of previous figures. Downwards arrows indicate upper limits. The solid black line is the threshold between poor and rich environments (CR=30), as indicated by Gendre et al. (2013). The dashed line represents the linear regression of data computed with ASURV parametric EM algorithm, including upper limits. The equation is: $\text{Log}(L_X/L_{\text{Edd}}) = -(0.022 \pm 0.005) \times CR - (3.8 \pm 0.3)$.

FRIIs (Godfrey & Shabala 2013). In particular, Cavagnolo et al. (2010b) concluded that a k-value larger than 100 is necessary to match with the relation proposed by Willott. Therefore, different classes of sources can require different values of f. We note that increasing f-values from FRIs to FRII-LERGs and FRII-HERGs/BLRGs could indeed mantain the proportionality between jet power and accretion luminosity.

Indeed, we note that the radio luminosity of a radio source can be amplified by radiative losses if the jet propagates through a dense environment. As claimed by Barthel & Arnaud (1996) on the basis of a Cygnus A study, this effect would amplify the radio luminosity and, in turn, weakens its reliability as estimator of the AGN power.

5 CONCLUSIONS

The comparison of the optical/X-ray luminosities, accretion rates, and intrinsic nuclear absorption between the three examined classes of sources (FRIs, FRII-LERGs, FRII-HERGs/BLRGs) have solidly established that FRII-LERGs have intermediate properties. The measurement of moderate gas column densities in FRII-LERGs, combined with a modest dust reddening, enables us to directly reject the first discussed scenario (see Section 4.1), in which FRII-LERGs are a highly obscured version of classical powerful FRIIs.

Instead, the moderate N_H column densities and X-ray/[OIII] luminosities are indicative of a weak nuclear activity with respect to the more obscured FRII-HERGs/BLRGs.

This leads at least to two different interpretations: i) FRII-LERGs are "starved" classical FRII-HERGs/BLRGs,

Table 3. Spectral parameters of the soft X-ray component.

Name	Γ_S	kT (keV)	$L_{0.5-2}$ (10^{42} erg s^{-1})
FRII-LERGs			
3C88	$1.6=\Gamma_H$	-	$0.03^{0.007}_{0.005}$
3C173.1	$1.7=\Gamma_H$	-	$0.3^{+0.3}_{-0.2}$
3C196.1	-	$3.2^{+1.3}_{-0.8}$	9 ± 1
3C288	-	$3.7^{+2.9}_{-1.2}$	$3.6^{+0.6}_{-0.5}$
3C310	-	1.0 ± 0.2	$0.04^{+0.01}_{-0.009}$
3C353	$1.7=\Gamma_H$	-	0.04 ± 0.01
3C357	$2=\Gamma_H$	-	$0.9^{+0.7}_{-0.3}$
3C388	-	$2.1^{+0.3}_{-0.2}$	$1.5^{+0.2}_{-0.1}$
3C460	$1.7 = \Gamma_H$	-	0.7 ± 0.3
FRII-HERGs/BLRGs			
3C33	$1.7=\Gamma_H$	-	$1.0^{+0.3}_{-0.2}$
3C61.1	1.2 ± 1.0	-	0.7 ± 0.4
3C79	$1.7=\Gamma_H$	-	$1.8^{+1.0}_{-0.7}$
3C135	2.2 ± 1.0	-	0.5 ± 0.2
3C180	$1.7=\Gamma_H$	-	$0.9^{+0.6}_{-0.4}$
3C184.1	$1.7=\Gamma_H$	-	0.7 ± 0.3
3C192	$1.7=\Gamma_H$	-	0.04 ± 0.01
3C223	$1.7=\Gamma_H$	-	1.4 ± 0.4
3C234	2.3 ± 0.5	-	7 ± 1
3C277.3	$1.7=\Gamma_H$	-	$0.31^{+0.1}_{-0.08}$
	$N_{H,2} = 1.1^{+0.5}_{-0.4}$ ‡		
3C285	$1.7=\Gamma_H$	-	0.14 ± 0.1
3C305	-	0.8 ± 0.2	$0.013^{+0.006}_{-0.005}$
3C321	2.8 ± 0.2	-	$0.8^{+0.07}_{-0.06}$
3C327	$1.7=\Gamma_H$	$0.20^{+0.04}_{-0.02}$	1.9 ± 0.1
3C379.1	$1.7=\Gamma_H$	-	$1.2^{+0.9}_{-0.7}$
3C381	$1.7=\Gamma_H$	-	$2. \pm 0.5$
3C403	$1.7=\Gamma_H$	0.20 ± 0.03	0.4 ± 0.04
3C436	$1.7=\Gamma_H$	-	0.4 ± 0.2
3C452	$1.7=\Gamma_H$	-	0.1 ± 0.04
3C459	$1.7=\Gamma_H$	$0.7^{+0.2}_{-0.1}$	$3.9^{+0.7}_{-0.6}$

‡ – a secondary absorption component is also required for this source (see Worrall et al. 2016).

or ii) they are a separate class of radio galaxies with their own properties.

In both cases, assuming a $P_{\text{jet}} - L_{\text{radio}}$ relation, FRII jets appear to carry out similar amount of energy independently on their optical classification (and different X-ray luminosities). This is difficult to explain within the paradigm that assumes powerful jets produced by efficient accretors.

In the former case, this apparent disagreement could be explained if FRII-LERGs are switching from an efficient to an inefficient regime and this information may not have reached the lobe-scales yet. In the latter case, the different trend of radio (jet power) and X-ray luminosities (accretion power) can be reconciled if the usually adopted $P_{\text{jet}} - L_{\text{radio}}$ relation does not properly take into account the jet interaction with the surrounding medium.

ACKNOWLEDGEMENTS

Table 4. Reprocessed Features.

Name	FeK_α line[a]	Reflection (R)
FRII-LERGs		
3C88	unconstrained	-
3C132	EW< 949	-
3C165	EW< 776	-
3C166	EW< 388	-
3C173.1	EW≥ 886	-
3C213.1	unconstrained	-
3C236	EW< 572	-
3C326	unconstrained	-
3C349	EW< 339	-
3C353	EW=100 ± 78	-
3C357	EW< 610	-
3C401	unconstrained	-
3C460	EW< 359	-
FRII-HERGs/BLRGs		
3C20	EW< 281	-
3C33	EW=139 ± 89	R=$1.5^{+0.4}_{-0.6}$
3C61.1	EW< 359	-
3C79	EW< 157	-
3C98	EW=277 ± 135	-
3C105	EW=178 ± 132	-
3C133	EW< 453	-
3C135	EW= 916^{+1474}_{-719}	-
3C171	EW< 117	-
3C180	EW< 744	-
3C184.1	EW< 278	-
3C192	EW< 260	-
3C223	EW< 836	-
3C223.1	EW< 374	-
3C234	EW= 900 ± 400	-
3C277.3	EW= 200 ± 100	-
3C284	unconstrained	-
3C285	EW=367^{+144}_{-47}	-
3C300	unconstrained	-
3C303.1	unconstrained	-
3C305	unconstrained	-
3C321	EW=988^{+751}_{-474}	-
3C327	EW=2000^{+3000}_{-742}	-
3C379.1	EW=557^{+1900}_{-464}	-
3C381	EW< 2304	-
3C403	EW=153^{+60}_{-15}	-
3C436	EW< 591	-
3C452	EW=172^{+65}_{-65}	R=$2^{+0.4}_{-0.5}$
3C456	EW< 156	-
3C458	EW< 238	-
3C459	EW< 649	-

[a] – Observed iron line equivalent width in eV.

REFERENCES

Abramowicz M. A., Chen X., Kato S., Lasota J.-P., Regev O., 1995, ApJ, 438, L37

Allen S. W., Dunn R. J. H., Fabian A. C., Taylor G. B., Reynolds C. S., 2006, MNRAS, 372, 21

Arnaud K. A., 1996, in Jacoby G. H., Barnes J., eds, Astronomical Society of the Pacific Conference Series Vol. 101, Astronomical Data Analysis Software and Systems V. p. 17

Avni Y., 1976, ApJ, 210, 642

Balmaverde B., Capetti A., Grandi P., 2006, A&A, 451, 35

Balmaverde B., et al., 2012, A&A, 545, A143

Barthel P. D., Arnaud K. A., 1996, MNRAS, 283, L45

Bennett A. S., 1962, Memoirs of the Royal Astronomical Society, 68, 163

Bianchi S., Guainazzi M., 2007, in di Salvo T., Israel G. L., Piersant L., Burderi L., Matt G., Tornambe A., Menna M. T., eds, American Institute of Physics Conference Series Vol. 924, The Multicolored Landscape of Compact Objects and Their Explosive Origins. pp 822–829 (arXiv:astro-ph/0611045), doi:10.1063/1.2774948

Bîrzan L., McNamara B. R., Nulsen P. E. J., Carilli C. L., Wise M. W., 2008, ApJ, 686, 859

Blandford R. D., Payne D. G., 1982, MNRAS, 199, 883

Blandford R. D., Znajek R. L., 1977a, MNRAS, 179, 433

Blandford R. D., Znajek R. L., 1977b, MNRAS, 179, 433

Bohlin R. C., Savage B. D., Drake J. F., 1978, ApJ, 224, 132

Burgess A. M., Hunstead R. W., 2006a, AJ, 131, 100

Burgess A. M., Hunstead R. W., 2006b, AJ, 131, 114

Buttiglione S., Capetti A., Celotti A., Axon D. J., Chiaberge M., Macchetto F. D., Sparks W. B., 2009, A&A, 495, 1033

Buttiglione S., Capetti A., Celotti A., Axon D. J., Chiaberge M., Macchetto F. D., Sparks W. B., 2010, A&A, 509, A6

Buttiglione S., Capetti A., Celotti A., Axon D. J., Chiaberge M., Macchetto F. D., Sparks W. B., 2011, A&A, 525, A28

Calzetti D., 1997, AJ, 113, 162

Capetti A., Massaro F., Baldi R. D., 2017, A&A, 601, A81

Cardelli J. A., Clayton G. C., Mathis J. S., 1989, ApJ, 345, 245

Cash W., 1979, ApJ, 228, 939

Cavagnolo K. W., McNamara B. R., Nulsen P. E. J., Carilli C. L., Jones C., Bîrzan L., 2010a, ApJ, 720, 1066

Cavagnolo K. W., McNamara B. R., Nulsen P. E. J., Carilli C. L., Jones C., Bîrzan L., 2010b, ApJ, 720, 1066

Celotti A., Padovani P., Ghisellini G., 1997, MNRAS, 286, 415

Evans D. A., Worrall D. M., Hardcastle M. J., Kraft R. P., Birkinshaw M., 2006, ApJ, 642, 96

Fabbiano G., Kim D. W., Trinchieri G., 1992, The Astrophysical Journal Supplement Series, 80, 531

Fanaroff B. L., Riley J. M., 1974, MNRAS, 167, 31P

Feigelson E. D., Nelson P. I., 1985, ApJ, 293, 192

Ferrarese L., Merritt D., 2000, ApJ, 539, L9

Gaskell C. M., 1982, PASP, 94, 891

Gaskell C. M., 1984, Astrophys. Lett., 24, 43

Gebhardt K., et al., 2000, ApJ, 539, L13

Gendre M. A., Best P. N., Wall J. V., Ker L. M., 2013, MNRAS, 430, 3086

Ghisellini G., 2010, in Bertin G., de Luca F., Lodato G., Pozzoli R., Romé M., eds, American Institute of Physics Conference Series Vol. 1242, American Institute of Physics Conference Series. pp 43–54 (arXiv:1002.4619), doi:10.1063/1.3460151

Ghisellini G., Haardt F., Matt G., 1994, MNRAS, 267, 743

Ghisellini G., Tavecchio F., Maraschi L., Celotti A., Sbarrato T., 2014, Nature, 515, 376

Godfrey L. E. H., Shabala S. S., 2013, ApJ, 767, 12

Gopal-Krishna Wiita P. J., 2000, A&A, 363, 507

Gordon K. D., Clayton G. C., Misselt K. A., Land olt A. U., Wolff M. J., 2003, ApJ, 594, 279

Grandi P., Malaguti G., Fiocchi M., 2006, ApJ, 642, 113

Greene J. E., Ho L. C., 2005, ApJ, 627, 721

Greene J. E., Ho L. C., 2006, ApJ, 641, L21

Heard C. Z. P., Gaskell C. M., 2016, MNRAS, 461, 4227

Heckman T. M., Best P. N., 2014, Annual Review of Astronomy and Astrophysics, 52, 589

Isobe T., Feigelson E. D., Nelson P. I., 1986, ApJ, 306, 490

Kalberla P. M. W., Burton W. B., Hartmann D., Arnal E. M., Bajaja E., Morras R., Pöppel W. G. L., 2005, A&A, 440, 775

Komatsu E., et al., 2009, ApJS, 180, 330

Kormendy J., 1993, in Dejonghe H., Habing H. J., eds, IAU Symposium Vol. 153, Galactic Bulges. p. 209

Kormendy J., 2004, in Ho L. C., ed., Coevolution of Black Holes and Galaxies. p. 1 (arXiv:astro-ph/0306353)

Kraft R. P., Azcona J., Forman W. R., Hardcastle M. J., Jones C., Murray S. S., 2006, ApJ, 639, 753

Kraft R. P., et al., 2012, ApJ, 749, 19

Laing R. A., Riley J. M., Longair M. S., 1983, MNRAS, 204, 151

Laing R. A., Jenkins C. R., Wall J. V., Unger S. W., 1994, in Bicknell G. V., Dopita M. A., Quinn P. J., eds, Astronomical Society of the Pacific Conference Series Vol. 54, The Physics of Active Galaxies. p. 201

Lal D. V., et al., 2010, ApJ, 722, 1735

Lightman A. P., White T. R., 1988, ApJ, 335, 57

Liu W., et al., 2019, MNRAS, 484, 3376

Magorrian J., et al., 1998, AJ, 115, 2285

Maraschi L., Tavecchio F., 2003, ApJ, 593, 667

Marconi A., Hunt L. K., 2003, ApJ, 589, L21

Massaro F., et al., 2010, ApJ, 714, 589

Massaro F., et al., 2012, The Astrophysical Journal Supplement Series, 203, 31

McConnell N. J., Ma C.-P., Gebhardt K., Wright S. A., Murphy J. D., Lauer T. R., Graham J. R., Richstone D. O., 2011, Nature, 480, 215

Merloni A., Heinz S., di Matteo T., 2003, MNRAS, 345, 1057

Momcheva I. G., Lee J. C., Ly C., Salim S., Dale D. A., Ouchi M., Finn R., Ono Y., 2013, AJ, 145, 47

Morganti R., Killeen N. E. B., Tadhunter C. N., 1993, MNRAS, 263, 1023

Narayan R., Yi I., 1994, ApJ, 428, L13

Narayan R., Mahadevan R., Grindlay J. E., Popham R. G., Gammie C., 1998, ApJ, 492, 554

Osterbrock D. E., 1989, Astrophysics of gaseous nebulae and active galactic nuclei

Padovani P., 2016, A&ARv, 24, 13

Rawlings S., Saunders R., 1991, Nature, 349, 138

Reynolds C. S., Brenneman L. W., Stocke J. T., 2005, MNRAS, 357, 381

Ricci F., et al., 2018, ApJ, 867, 35

Risaliti G., 2002, A&A, 386, 379

Shakura N. I., Sunyaev R. A., 1973, A&A, 500, 33

Sikora M., Stawarz Ł., Lasota J.-P., 2007, ApJ, 658, 815

Spinrad H., Djorgovski S., Marr J., Aguilar L., 1985, Publications of the Astronomical Society of the Pacific, 97, 932

Tadhunter C., 2016, Astronomy and Astrophysics Review, 24, 10

Tremaine S., et al., 2002, ApJ, 574, 740

Tsvetanov Z. I., Iankulova I. M., 1989, MNRAS, 237, 707

Wall J. V., Peacock J. A., 1985, MNRAS, 216, 173

Willott C. J., Rawlings S., Blundell K. M., Lacy M., 1999, MNRAS, 309, 1017

Wing J. D., Blanton E. L., 2011, AJ, 141, 88

Worrall D. M., Birkinshaw M., Young A. J., 2016, MNRAS, 458, 174

Wysota A., Gaskell C. M., 1988, Reddening of Narrow Line Regions. pp 79–82, doi:10.1007/3-540-19492-4_171